Terahertz electroluminescence from superlattice quantum cascade structures

Raffaele Colombelli, Axel Straub, Federico Capasso, Claire Gmachl, Myrtle I. Blakey, A. Michael Sergent, S. N. George Chu, Ken W. West, and Loren N. Pfeiffer
Bell Laboratories, Lucent Technologies, 600 Mountain Avenue, Murray Hill, New Jersey 07974

(Received 26 July 2001; accepted for publication 7 December 2001)

Intersubband electroluminescence is reported in a quantum-cascade structure based on asymmetric superlattice active regions and designed for emission in the THz range (λ≈80 μm). Comparison with a structure based on a "vertical transition" in a single quantum well shows an increased full width at half maximum (2.8 vs 0.9 meV) of the emission line. In both cases the dependence of the optical power on the injected current is linear or sublinear and remains in the pW range. © *2002 American Institute of Physics.* [DOI: 10.1063/1.1448393]

Since their invention in 1994,[1] quantum cascade (QC) lasers have seen constant innovation as tunable coherent sources in the mid-infrared (mid-IR) range of the electromagnetic spectrum.[2,3] Research in this field is continuously expanding: new material systems are being explored,[4] ultrahigh-speed operation and mode locking have been demonstrated,[5] and new spectral ranges outside the mid-IR are under investigation.[6,7] The demonstration of a semiconductor injection laser at very long wavelengths would be of great importance due to the present lack of convenient and compact sources. Considerable progress has been made in the range between 20 and 30 μm wavelength;[8] laser action in the THz range, however, on the lower-energy side of the Reststrahlenband (λ⩾50 μm) of commonly used materials such as GaAs or InP based semiconductors, has not yet been achieved.[9]

There are two main components to semiconductor laser action: a low-loss waveguide resonator with large optical confinement, and gain, which is conveniently derived from population inversion.

First, the waveguide of choice at long wavelengths is based on surface plasmons, i.e., the mode is guided by a metal/semiconductor interface instead of the refractive index contrast within a thick stack of semiconductor lasers.[10] This results in a substantially reduced thickness of the epitaxially grown material, and in a significant increase of the mode confinement factor. Ideally, at THz frequencies, the waveguide should be based on a metal-semiconductor-metal geometry, but fabrication difficulties suggest that replacing the bottom metal with a highly doped n^{++} semiconductor layer is a more convenient strategy. A QC laser device based on this waveguide configuration has been recently demonstrated at a wavelength of 21.5 μm.[8] The optical loss at THz frequencies of such a waveguide was recently measured by Rochat *et al.*[11] at λ≈75 μm by mean of a multisection single-pass technique. They found a value $\alpha_w = 42 \pm 20\,\mathrm{cm}^{-1}$, in agreement with calculations based on free-carrier absorption.

Achieving population inversion is another essential step for the realization of a THz QC laser. At THz frequencies the photon energy is smaller than the typical optical phonon energies (~34/36 meV). Thus LO-phonon scattering is no longer an effective way to obtain population inversion, contrary to the case of mid-IR QC lasers. This is because it is difficult to selectively empty the lower laser state by resonant LO-phonon scattering without—at the same time—removing carriers from the excited state. In addition the electron-electron $(e-e)$ scattering rate scales approximately as ΔE^{-1}, where ΔE is the energy separation between the states. Therefore, it can become the dominant scattering process,[12,13] at least for electrons which do not carry enough kinetic energy to emit an LO phonon. The complexity of the mechanisms involved in $e-e$ scattering is well confirmed by the different values reported in the literature[14] for the intersubband nonradiative scattering times, which range from subpicosecond times to a few nanoseconds. Electron-electron scattering must therefore be taken into account in designing THz QC lasers, or it may be taken advantage of.[15]

A SL active region structure is the simplest design that could benefit from $e-e$ scattering. The radiative transition is across the minigap between two manifolds of extended states (minibands). Due to the ΔE^{-1} dependence of the $e-e$ scattering rate[12,13] the intraminiband scattering rates can be made in principle several times higher than the interminiband ones,[13] e.g., when the distance between the states in the SL miniband is 2–4 meV, while the minigap is ≈15 meV (λ =82.5 μm). This characteristic, although not relevant for electroluminescence, is very important for lasing, since it can give rise to an intrinsic population inversion. Finally, a SL-based design facilitates the flow of high currents, overcoming the problem of very low current densities which is typical of single QW based active regions.[7] While in a SL based active region the nonradiative scattering rates are stronger due to the larger number of possible transitions, leading to higher threshold current densities for laser action, this increase is compensated by the possibility of driving the devices at much higher currents, as stated above.

In this letter, we report THz electroluminescence (EL) from a SL QC structure and compare it with the case of a two-level single QW structure. We stress that this is the first experimental demonstration of a superlattice active region Terahertz emitter, while all previous such demonstrations

 © 2002 American Institute of Physics

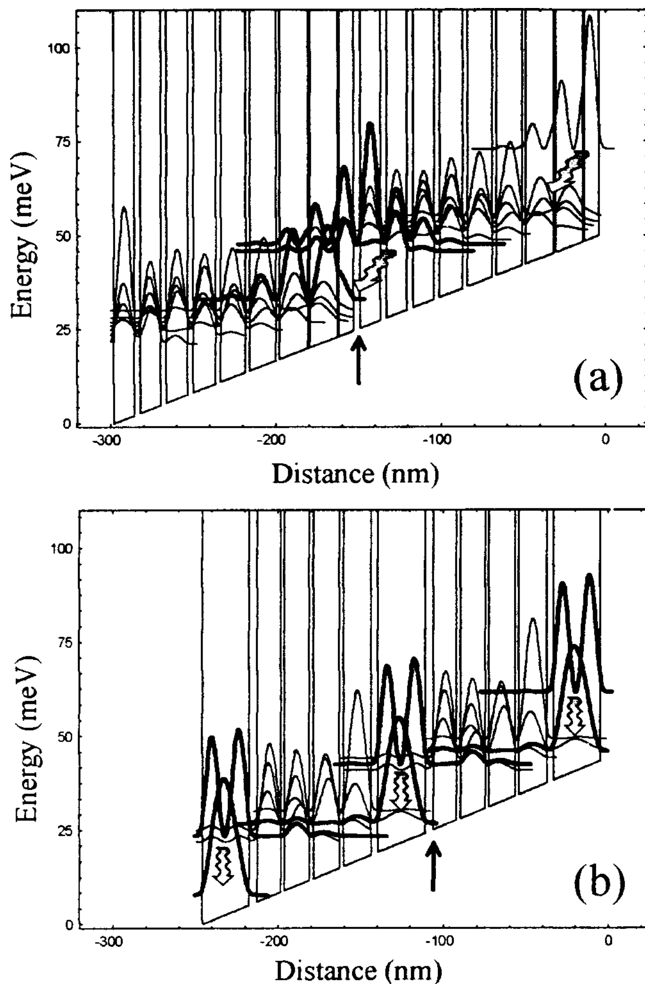

FIG. 1. (a) Conduction-band profile of two periods of sample 𝒜, under an applied electric field of 1.7 kV/cm. The layer thicknesses in nm of a single stage are, from left to right, starting from the barrier marked by an arrow: **4.2**/12/**3.7**/12.4/**3.6**/13/**3.2**/13.9/**3.0**/14.8/**2.5**/15.9/**2.0**/17.3/**1.0**/16.9/**0.6**/9. AlGaAs barriers are in boldface. Underlined layers are doped with Si to $2\times10^{16}\,\mathrm{cm}^{-3}$. The moduli squared of the relevant wave functions are shown; the wavy arrows indicate the radiative transition, designed for emission at $\lambda=84\ \mu$m. (b) Conduction-band profile for sample ℬ, under an electric field of 1.8 kV/cm. The layer thicknesses in nm are, starting from the injection barrier: **4.8**/14/**2.3**/15/**2.3**/16/**2.3**/17/**4.0**/28.5. Underlined layers are doped to $1\times10^{16}\,\mathrm{cm}^{-3}$. The radiative transition, indicated by wavy arrows, was designed at $\lambda=80\ \mu$m.

were based on single quantum well structures.[7] Our SL structure (sample 𝒜) was grown by molecular beam epitaxy using a $GaAs/Al_{0.15}Ga_{0.85}As$ lattice matched to a highly-doped ($n\sim2\times10^{18}\,\mathrm{cm}^{-3}$) GaAs substrate. The active region is based on an interminiband transition in an asymmetric superlattice [Fig. 1(a)]. The SL character of this optical transition is determined by the relatively large number of QWs (~6) over which the wave functions are delocalized. The active region was repeated 40 times. It was preceded by the growth of a 1-μm-thick highly doped ($n\sim7\times10^{18}\,\mathrm{cm}^{-3}$) GaAs layer, which acts as the n^{++} plasma layer, and is followed by a contact facilitating layer (150 nm of GaAs doped to $n\sim2\times10^{18}\,\mathrm{cm}^{-3}$). Two other structures (samples ℬ and ℬ′), based on an intrawell transition between two well-localized states in a single QW, were grown for comparison (Figs. 1(b) and 3(c)) for layer thicknesses) with similar cladding layers, but on an insulating GaAs substrate. In sample ℬ, the spontaneous emission takes place between the excited and the ground state of a wide quantum well. The calculated optical dipole matrix element is $z=5.1$ nm. In sample 𝒜 instead, the optical transition involves states delocalized on several wells [Fig. 1(a)], and the matrix element is $z=5.7$ nm. In addition, while structure ℬ relies mainly on tunneling to extract carriers from the ground state, sample 𝒜 relies instead on intraminiband scattering inside the lower miniband.

The samples were processed into $400\times400\ \mu\mathrm{m}^2$ mesas. Ge/Au/Ti/Pt/Au contacts were deposited on top and were later annealed at a temperature of 420 °C. Contacts are metal gratings with a period ranging from 10 to 20 μm, but the mesa were cleaved in the middle to allow light extraction from the facet. Devices were then soldered with indium to a copper block, wire bonded, and mounted in an He-flow cryostat for the measurements. The light collected by a parabolic mirror was spectrally analyzed in a Nicolet Fourier transform infrared spectrometer equipped with a He-cooled Si bolometer or a doped-Ge detector. Due to the low speed of the detectors, the devices were driven with bursts of 605 1.5-μs-wide pulses. The burst frequency was 413 Hz, which corresponds to an overall duty cycle of 37.5%. All the measurements were performed with the FTIR operating in step-scan mode.

Figure 2(a) shows typical EL spectra taken at cryogenic temperatures for sample 𝒜. The emission consists of a single line centered at a wavelength of 82 μm (15 meV), very close to the design wavelength of 84 μm (14.7 meV), with a full width at half maximum (FWHM) of ~2.8 meV and constant with current. The emission appears first at an injected current of ~150 mA, and at an applied voltage reasonably close to the design bias of 1 V. This value corresponds to the electric field of 1.7 kV/cm [Fig. 2(b)]. The emission peak increases with current and for values $\geqslant$350 mA a broad shoulder rises at the low-energy side of the peak, which we attribute to thermally generated blackbody emission. A sudden increase in differential resistance (most probably indicating domain formation) appears above 500 mA in the current-voltage characteristic, above which the thermal background completely dominates over the optical emission from the SL [see Fig. 2(a), upper spectrum at 550 mA driving current]. The attribution of the low-energy shoulder to thermal background, which is not surprising given the high duty cycle used in these measurements (almost 40%), should be clear following its evolution in Fig. 2(a) in the last four spectra, at currents ranging from 350 to 550 mA. The low-energy shoulder is not a peak, but it is a low-energy background spectrum convoluted with the detector frequency response, which has a cutoff at about 9 meV, marked by the dashed vertical line in Fig. 2(a). Above the region of high differential resistance, the sudden increase in applied voltage leads to a sudden increase in dissipated power too, thus explaining why the thermal background completely dominates. Figure 2(c) shows the integrated luminescence intensity of the emission at $\lambda\approx82\ \mu$m as a function of injected current. The char-

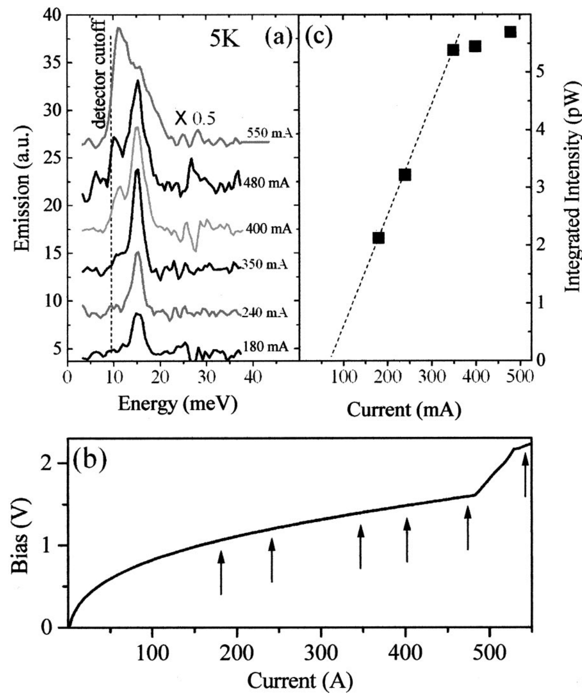

FIG. 2. (a) THz electroluminescence (EL) at 5 K of sample $\mathscr{A}$, measured at different currents as indicated. The emission at 15 meV ($\lambda \approx 82$ μm), is close in energy to the designed value of 14.7 meV ($\lambda = 84$ μm). The dashed line marks the detector (an He-cooled doped-Germanium) cutoff energy. (b) Current-voltage ($I-V$) characteristic of the device. The arrows mark the current values where optical spectra were measured. At 500 mA a sudden increase in differential resistance appears, and the thermal background starts to dominate the optical emission. (c) PL intensity vs injected current at 5 K.

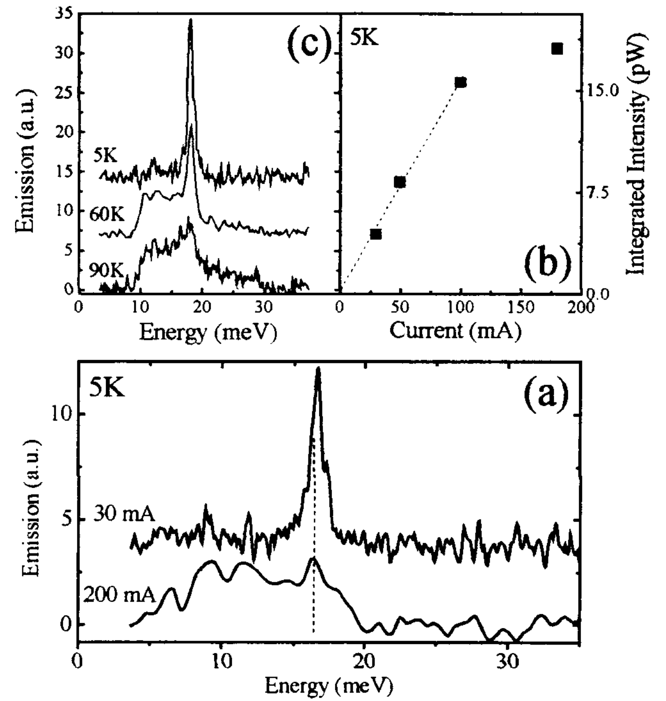

FIG. 3. (a) THz EL at 8 K of sample $\mathscr{B}$, measured at 30 mA injected current (below the region of high differential resistance) and at 200 mA. In the latter the thermal background completely dominates the emission. (b) PL intensity vs injected current at 8 K for sample $\mathscr{B}$. (c) THz EL of sample $\mathscr{B}'$ at different heat sink temperatures. Sample $\mathscr{B}'$ is a copy of sample $\mathscr{B}$ with a 10% reduction in all layers thicknesses (barriers and wells).

acteristic is linear up to 350 mA, showing that in this range the luminescence efficiency is constant, then it saturates visibly, the origin of which is not yet understood. The linear fit below 350 mA [dashed line in Fig. 2(b)] does not intercept the origin. The reason is that the emission is due to an interminiband transition, so that no emission can occur before the structure is energetically aligned.

Figure 3(a) shows EL spectra taken at cryogenic temperatures for sample $\mathscr{B}$, based on the intrawell transition. The spectrum at 30 mA shows a very narrow emission line (FWHM ~0.9 meV, not limited by the instrument resolution) centered at 74.5 μm (16.6 meV), reasonably close to the design wavelength of 80 μm (15.5 meV). At 200 mA instead (in the region of very high differential resistance) the peak is again barely visible beneath a broad thermal background. The integrated EL intensity of the same sample as a function of current is shown in Fig. 3(b). The characteristic is linear up to 100 mA and then saturates, but contrary to sample $\mathscr{A}$ the linear fit intercepts the origin.

The two designs exhibit emissions with different FWHM, in particular the EL from sample $\mathscr{A}$ (FWHM=2.8 meV) is approximately three times broader than the one from sample $\mathscr{B}$ (FWHM=0.9 meV). Since in both cases the line broadening is expected to be inhomogeneous, the result is in good agreement with the characteristics of the samples. SL-based structures usually exhibit broader FWHM due to the higher number of interfaces and increased interface roughness scattering. According to a standard formula for the threshold current density in QC lasers[16] broader lines imply higher thresholds, but this effect is usually compensated by higher gain and by the possibility of injecting higher currents in a SL structure. In our case, in fact, the EL intensity saturates at 125 A/cm^2 in sample $\mathscr{B}$, based on a intrawell transition, while in the structure based on the interminiband transition the saturation occurs at the much higher current density of 450 A/cm^2.

The estimated integrated maximum optical power emitted by our structures is 5 and 15 pW, respectively, for samples $\mathscr{A}$ and $\mathscr{B}$. This is somewhat surprising, since the optical dipole matrix element is slightly bigger for the SL-based sample. A possible explanation comes from the analysis of the nonradiative scattering rates. The optical power for spontaneous emission is related to the injected current by the following formula, which is independent of the nature of the nonradiative scattering process. It therefore includes both LO-phonon scattering and electron-electron scattering (and potentially other scattering mechanisms):

$$P_{\mathrm{opt}} = \eta_{\mathrm{coll}} N \hbar \omega \frac{I}{e} \frac{\Gamma_{\mathrm{rad}}}{\Gamma_{\mathrm{non\text{-}rad}}}, \tag{1}$$

where η_{coll} is the overall collection efficiency (which includes the effectiveness of light extraction from the cleaved mesa), N the number of stages, $\hbar\omega$ the transition energy, I the injected current, Γ_{rad} the radiative, and $\Gamma_{\mathrm{non\text{-}rad}}$ the nonradiative scattering rates, respectively. Assuming identical collection efficiency we obtain an upper limit for the ratio between the scattering times in the two samples of 10, i.e., the

nonradiative intersubband scattering rate should be at most 10 times faster in sample $\mathscr{A}$, based on a SL, than in sample $\mathscr{B}$, based on a QW.

A number of possible reasons can be found for this result. First, while in sample $\mathscr{B}$ the excited state of the radiative transition is localized, and carriers can essentially scatter only to the ground state, in sample $\mathscr{A}$ carriers have access to all the states of the lower miniband and the number of scattering channels increases almost by an order of magnitude. This can affect, in particular, hot electrons with enough kinetic energy to emit an LO phonon and thus scatter to lower-energy states with subpicosecond times.

In addition the nominal doping levels of the two samples are quite different ($1\times10^{11}\,\mathrm{cm}^{-2}$ for sample $\mathscr{A}$, $3.5\times10^{10}\,\mathrm{cm}^{-2}$ for sample $\mathscr{B}$). Electron-electron scattering is the main scattering process at energies below the LO phonon, and it depends on doping in a nonstraightforward way;[12–14] such a difference in electron concentration can affect the nonradiative rates of the system.

The different doping levels of the samples can explain their different temperature behavior. The emission from the SL structure is completely broadened already at 60 K (data not shown). Sample $\mathscr{B}'$ instead exhibits a sharp line at the same temperature, with no discernible broadening, with a superimposed blackbody background [see Fig. 3(c)]. Only at a heat sink temperature of 90 K the thermal background dominates over the emission peak from the QW.

In conclusion, we reported THz EL in a QC structure with asymmetric superlattice active regions and we compared it with emission from a sample based on a vertical transition. The latter exhibits a narrower emission line, but the former is able to carry more injected current at constant luminescence efficiency, an important feature in order to achieve population inversion. We have finally estimated a higher nonradiative intersubband scattering rate for the sample based on a asymmetric-superlattice active region.

The authors would like to thank Michael C. Wanke for his help in the early stages of this work. This material is based upon work supported in part by DARPA/ARO under Contract No. DAAD19-00-C-0096.

[1] J. Faist, F. Capasso, D. L. Sivco, C. Sirtori, A. L. Hutchinson, and A. Y. Cho, Science **264**, 553 (1994).
[2] F. Capasso, R. Colombelli, R. Paiella, C. Gmachl, A. Tredicucci, D. L. Sivco, and A. Y. Cho, Opt. Photonics News **12**, 40 (2001); C. Gmachl, F. Capasso, R. Köhler, A. Tredicucci, A. L. Hutchinson, D. L. Sivco, J. N. Baillargeon, and A. Y. Cho, IEEE Circuits Devices Mag. **16**, 10 (2000); F. Capasso, C. Gmachl, A. Tredicucci, A. L. Hutchinson, D. L. Sivco, and A. Y. Cho, Opt. Photonics News **10**, 31 (1999).
[3] D. Hofstetter, M. Beck, T. Aellen, J. Faist, U. Oesterle, M. Ilegems, E. Gini, and H. Melchior, Appl. Phys. Lett. **78**, 1964 (2001).
[4] C. Sirtori, P. Kruck, S. Barbieri, P. Collot, J. Nagle, M. Beck, J. Faist, and U. Oesterle, Appl. Phys. Lett. **73**, 3486 (1998).
[5] R. Paiella, F. Capasso, C. Gmachl, C. G. Bethea, D. L. Sivco, J. N. Baillargeon, A. L. Hutchinson, A. Y. Cho, and H. C. Liu, IEEE Photonics Technol. Lett. **12**, 780 (2000); R. Paiella, F. Capasso, C. Gmachl, D. L. Sivco, J. N. Baillargeon, A. L. Hutchinson, A. Y. Cho, and H. C. Liu, Science **290**, 1739 (2000).
[6] C. Gmachl, H. M. Ng, and A. Y. Cho, Appl. Phys. Lett. **77**, 334 (2000).
[7] M. Rochat, J. Faist, M. Beck, U. Oesterle, and M. Ilegems, Appl. Phys. Lett. **73**, 3724 (1998); B. S. Williams, B. Xu, Q. Hu, and M. R. Melloch, *ibid.* **75**, 2927 (1999); J. Ulrich, R. Zobl, W. Schrenk, G. Strasser, K. Unterrainer, and E. Gornik, *ibid.* **77**, 1928 (2000).
[8] R. Colombelli, F. Capasso, C. Gmachl, A. L. Hutchinson, D. L. Sivco, A. Tredicucci, M. C. Wanke, A. M. Sergent, and A. Y. Cho, Appl. Phys. Lett. **78**, 2620 (2001).
[9] M. A. Odnoblyudov, I. N. Yassievich, M. S. Kagan, Yu. M. Galperin, and K. A. Chao, Phys. Rev. Lett. **83**, 644 (1999).
[10] C. Sirtori, C. Gmachl, F. Capasso, J. Faist, D. L. Sivco, A. L. Hutchinson, and A. Y. Cho, Opt. Lett. **23**, 1366 (1998).
[11] M. Rochat, M. Beck, J. Faist, and U. Oesterle, Appl. Phys. Lett. **78**, 1967 (2001).
[12] P. Hyldgaard and J. W. Wilkins, Phys. Rev. B **53**, 6889 (1996).
[13] P. Harrison, R. W. Kelsall, K. Donovan, and P. Kinsler, IEEE Trans. Microwave Theory Tech. **48**, 645 (2000).
[14] M. Hartig, S. Haacke, P. E. Selbmann, B. Deveaud, R. A. Taylor, and L. Rota, Phys. Rev. Lett. **80**, 1940 (1998); M. Hartig, J. D. Ganière, P. E. Selbmann, B. Deveaud, and L. Rota, Phys. Rev. B **60**, 1500 (1999); K. Kempa, P. Bakshi, J. Engelbrecht, and Y. Zhou, *ibid.* **61**, 11 083 (2000); K. W. Sun, C. K. Sun, J. C. Wang, S. Y. Wang, and C. P. Lee, Solid State Commun. **115**, 329 (2000).
[15] L. E. Vorob'ev, JETP Lett. **71**, 511 (2000).
[16] A. Tredicucci, F. Capasso, C. Gmachl, D. L. Sivco, A. L. Hutchinson, and A. Y. Cho, Appl. Phys. Lett. **73**, 2101 (1998).

Journal of Applied Physics is copyrighted by the American Institute of Physics (AIP). Redistribution of journal material is subject to the AIP online journal license and/or AIP copyright. For more information, see http://ojps.aip.org/japo/japcr/jsp
Copyright of Journal of Applied Physics is the property of American Institute of Physics and its content may not be copied or emailed to multiple sites or posted to a listserv without the copyright holder's express written permission. However, users may print, download, or email articles for individual use.